

## Fabrication of Flexible Microsupercapacitors with Binder-Free ZIF-8 Derived Carbon Films *via* Electrophoretic Deposition

Yang Li,<sup>1,2,3,4,#</sup> Joel Henzie,<sup>\*4</sup> Teahoon Park,<sup>5,#</sup> Jie Wang,<sup>4,#</sup> Christine Young,<sup>4</sup> Huaqing Xie,<sup>1,2,3</sup> Jin Woo Yi,<sup>5</sup> Jing Li,<sup>1,2,3</sup> Minjun Kim,<sup>6</sup> Jeonghun Kim,<sup>6</sup> Yusuke Yamauchi,<sup>\*6,7</sup> and Jongbeom Na<sup>\*4,6</sup>

<sup>1</sup>School of Environmental and Materials Engineering, College of Engineering, Shanghai Polytechnic University, Shanghai 201209, P. R. China

<sup>2</sup>Shanghai Innovation Institute for Materials, Shanghai 200444, P. R. China

<sup>3</sup>Research Center of Resource Recycling Science and Engineering, Shanghai Polytechnic University, Shanghai 201209, P. R. China

<sup>4</sup>International Center for Materials Nanoarchitectonics (WPI-MANA), National Institute for Materials Science (NIMS), 1-1 Namiki, Tsukuba, Ibaraki 305-0044, Japan

<sup>5</sup>Carbon Composite Department, Composites Research Division, Korea Institute of Materials Science (KIMS), 797, Changwon-daero, Seongsan-gu, Changwon-si, Gyeongsangnam-do, 51508, South Korea

<sup>6</sup>School of Chemical Engineering and Australian Institute for Bioengineering and Nanotechnology (AIBN), The University of Queensland, Brisbane, Queensland 4072, Australia

<sup>7</sup>Department of Plant and Environmental New Resources, Kyung Hee University, 1732 Deogyong-daero, Giheung-gu, Yongin-si, Gyeonggi-do 446-701, South Korea

E-mail: HENZIE.Joeladam@nims.go.jp (J. Henzie), y.yamauchi@uq.edu.au (Y. Yamauchi), j.na@uq.edu.au (J. Na)

Received: October 23, 2019; Accepted: October 31, 2019; Web Released: November 7, 2019

### Prof. Yusuke Yamauchi

Prof. Yusuke Yamauchi received his bachelor's degree (2003), master degree (2004), and a Ph.D. degree (2007) from Waseda University (Japan). After that, he joined NIMS to start his research group. In 2017, he moved to Australia to join The University of Queensland. Currently, he is a full professor at School of Chemical Engineering and a senior group leader at AIBN. He concurrently serves as an honorary group leader of NIMS, a visiting professor at several universities, and an associate editor of the Journal of Materials Chemistry A. He has published more than 750 papers in international refereed journals with >35,000 citations (*h*-index > 100). He has been selected as a Highly Cited Researcher in Chemistry in 2016, 2017, 2018, and 2019. He has received many outstanding awards, such as the NISTEP Award by National Institute of Science and Technology Policy (2016), the Chemical Society of Japan (CSJ) Award for Young Chemists (2014), the Young Scientists' Prize of the Commendation for Science and Technology by MEXT (2013), the PCCP Prize by the Royal Society of Chemistry (2013), the Tsukuba Encouragement Prize (2012), the Ceramic Society of Japan (CerSJ) Award (2010), and the Inoue Research Award for Young Scientists (2010). Recently, he was selected as one of Australia's Top 40 Researchers.



### Dr. Jongbeom Na

Dr. Jongbeom Na received his Ph.D. degree (2017) from the Department of Chemical and Biomolecular Engineering at Yonsei University (Republic of Korea). Until 2018, he worked as a Research Engineer at Chemical Laboratory of SK Chemicals Co., Ltd. Currently, he is working as a research fellow at MANA, NIMS (Japan) and as a visiting academic at AIBN, the University of Queensland. His major research interest is in the design and synthesis of functional nanomaterials, organic-inorganic hybrid materials, and energy conversion-storage applications.



### Abstract

Miniaturized power supplies, such as microsupercapacitors, are highly demanded in micro-electro mechanical systems (MEMS) and micro portable microdevices due to their superior

cyclability, high power density, and considerable energy. In this study, we utilize ZIF-8 derived carbon as a source of active material to fabricate flexible microsupercapacitors *via* a simple electrophoresis method. The deposited ZIF-8 derived carbon

particles with high surface area play a decisive role in achieving high electrochemical performances. The simple and straightforward process of electrophoretic deposition using ZIF-8 derived carbon particles generates porous carbon films on microsupercapacitors, which leads to a superior electrochemical performance.

**Keywords:** Nanoporous carbons | Porous materials | Metal-organic frameworks

## 1. Introduction

The advance of technologies in micro-electro-mechanical systems (MEMS) and portable microdevices has realized the integration of various technologies in miniaturized electronic devices. It has allowed an enormous degree of freedom and convenience towards a variety of applications such as environmental monitoring systems, biosensors, wearable sensors, and flexible displays.<sup>1–5</sup> However, the development of smart applications and technologies with MEMS and portable microdevices is limited by the lack of energy storage technologies. Therefore, efficient energy storage systems are required to increase the working period of microdevices.

Micro-supercapacitors (MSCs) can miniaturize energy storage devices that are highly useful to supply required electrical energy to microdevices as they possess high capacitance, large energy-density, and superior charge/discharge rates.<sup>6–9</sup> MSCs work based on the same type of electric charge storage mechanisms a traditional supercapacitors, which are known as electric double-layer capacitors (EDLCs)<sup>10,11</sup> and pseudocapacitors.<sup>12,13</sup> EDLCs store electrical charge *via* electrostatic adsorption/desorption of electrolyte ions along the interfaces between electrode and electrolyte, whereas pseudocapacitors store electrical charge *via* surface redox reaction of electrode materials. Among various electrode materials, nanoporous carbon materials can have high surface areas and good electrical conductivities, which enables their high specific capacitance *via* EDLC.

Metal-organic frameworks (MOFs) are highly porous and ordered materials formed *via* coordination bonding between metal ions and organic ligands.<sup>14,15</sup> With their organic ligands acting as carbon precursors, specific MOFs can give rise to highly porous carbons upon high annealing temperature.<sup>16–22</sup> ZIF-8 (zeolitic imidazolate framework-8) is one of the most commonly utilized MOF species to produce porous ZIF-8 derived carbon with a high surface area. Herein, we fabricate a microsupercapacitor deposited with ZIF-8 derived carbons as active materials *via* an electrophoretic deposition method (Figure 1a). The electrophoretic deposition method enables binder-free and conductive area-specific fabrication of micro-supercapacitors, which is hard to achieve with traditional drop-casting methods. Here we describe the fabrication of flexible microsupercapacitors and investigate their performance as energy storage devices. As a result, they exhibit high power density and high energy density with an outstanding capacitance retention rate.

## 2. Experimental

### 2.1 Synthesis of Carbon Particles of Two Different Diameters Derived from ZIF-8 Particles.

The reagents

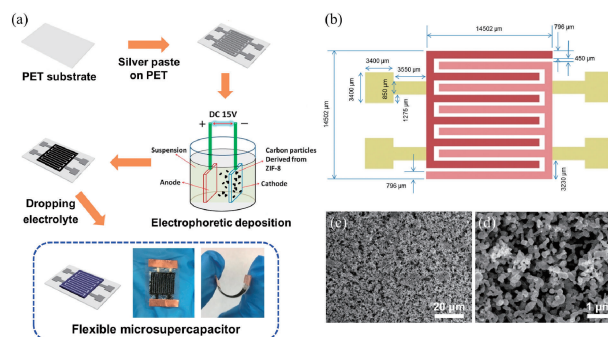


**Figure 1.** (a) Schematic of microsupercapacitor fabrication *via* electrophoretic deposition, (b) schematic of flexible interdigital finger electrode, and (c, d) SEM images of deposited carbon particles on the patterned lines.

and chemicals for ZIF-8 synthesis in the present study were purchased from Sigma-Aldrich company and utilized without any further treatment. In a typical synthesis method, 18.94 g (100 mmol) of  $\text{Zn}(\text{NO}_3)_2 \cdot 6\text{H}_2\text{O}$  was dissolved in 500 mL distilled water and dissolved adequately to obtain a clear solution. Then, 2-methylimidazole (MIm) was added in the above solution and continuously stirred. The mole ratio of  $\text{Zn}(\text{NO}_3)_2 \cdot 6\text{H}_2\text{O}$  and MIm was controlled at 1:70 and 1:50 to prepare different size ZIF-8 particles (average 350 nm and 1400 nm, respectively) for 24 h. As-prepared ZIF-8 particles were collected by centrifugation and washed with distilled water and ethanol several times. Finally, the ZIF-8 particles were dried at 50 °C under vacuum in an incubator for 24 h. For carbonization, as-synthesized ZIF-8 particles were placed into a porcelain boat in the tube furnace and pyrolyzed at 800 °C for 5 h, with a heating rate of 5 °C·min<sup>-1</sup> in N<sub>2</sub> atmosphere, resulting in ZIF-8 derived carbon particles. Hereafter, the carbon particles of two different sizes are denoted as C350 and C1400, according to the size of ZIF-8 particles, *ca.* 350 nm and *ca.* 1400 nm, respectively.

**2.2 Fabrication of a Supercapacitor by Electrophoretic Deposition.** A three-electrode setup was used to initially evaluate the electrochemical properties of C350 and C1400 as active materials for supercapacitors. Then flexible microsupercapacitors were fabricated to assess device performances.

**Three-Electrode Supercapacitor:** Polyethylene terephthalate (PET) was selected as the substrate for a supercapacitor due to its flexibility and chemical stability in most cases. Before electrophoretic deposition, PET substrates were coated with silver paste by brush and subsequent drying at 150 °C for 10 min. The C350 and C1400 particles were combined with a suspension containing carbon particles to conduct electrophoretic deposition. It was prepared as follows: Carbon particles (0.2% wt.) and  $\text{Mg}(\text{NO}_3)_2 \cdot 6\text{H}_2\text{O}$  (0.02% wt.) were suspended in distilled water-ethanol mixed solution (95%:5%). The suspension was sonicated for 8 h to disperse carbon particles sufficiently. As a result, the suspension could remain stable for seven days without precipitate at the bottom of the suspension, which ensured the colloidal suspension was stable. The electrophoresis was carried out in a two-electrode system with the suspension functioning as the electrolyte. The PET substrate and Pt foil were employed as anode and cathode during electrophoretic deposition. In a typical deposition experiment, 15 V

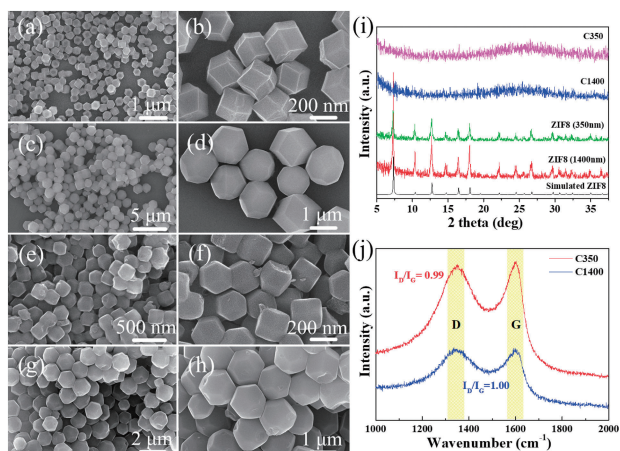


**Figure 2.** (a–d) SEM images of two types of as-prepared ZIF-8 particles with different particle sizes of (a, b) *ca.* 350 nm and (c, d) *ca.* 1400 nm. (e–h) SEM images of ZIF-8 derived carbon particles with different particle sizes ((e, f) C350 and (g, h) C1400). (i) Wide-angle XRD patterns of as-prepared ZIF-8 particles with different particle sizes and ZIF-8 derived carbon particles (C350 and C1400). (j) Raman spectra of ZIF-8 derived carbon particles (C350 and C1400).

was applied between anode and cathode for 1 min. Then deposited PET substrate was taken out to be washed with distilled water and dried at 60 °C for 50 min to obtain a binder-free electrode.

**Flexible Microsupercapacitor:** The illustration in Figure 1a describes the fabrication method used to create the flexible microsupercapacitors. The electrophoretic deposition process of the electrodes for flexible microsupercapacitor was the same as the above section, except that the electrode pattern was deposited on the PET substrate by applying silver paste through a screen-printing mask. The final interdigitated finger electrode figure can be seen in Figure 1b, which is denoted as flexible microsupercapacitor (FSC) after dropping of electrolyte.

**2.3 Materials Characterizations.** X-ray diffraction (XRD, Rigak, Cu  $K\alpha$  radiation) was used to determine the structures of ZIF-8 and its derived carbon particles. The morphology of as-prepared particles was examined by scanning electron microscopy (SEM, Hitachi, S-4800). The nitrogen adsorption-desorption isotherms were conducted by utilizing a surface area analysis apparatus (BET, Quantachrome Instruments, AUTOSORB-1) at 77 K to analyze the surface areas and pore size distribution of carbon particles. Micro-Raman spectrometer with a 633 nm laser source (Horiba-Jobin Yvon T64000) was used to study the carbon-related information of carbon particles.

**2.4 Electrochemical Measurements. Three-Electrode Supercapacitor:** All electrochemical measurements were carried out on an electrochemical workstation (VMP3, Biological, France). To measure the electrochemical performance of C350 and C1400 deposited PET electrodes, three electrode system was utilized, with 6 M KOH solution as the electrolyte, Pt foil as counter electrode and Ag/AgCl as the reference electrode. Cyclic voltammetry (CV) curves were measured within the

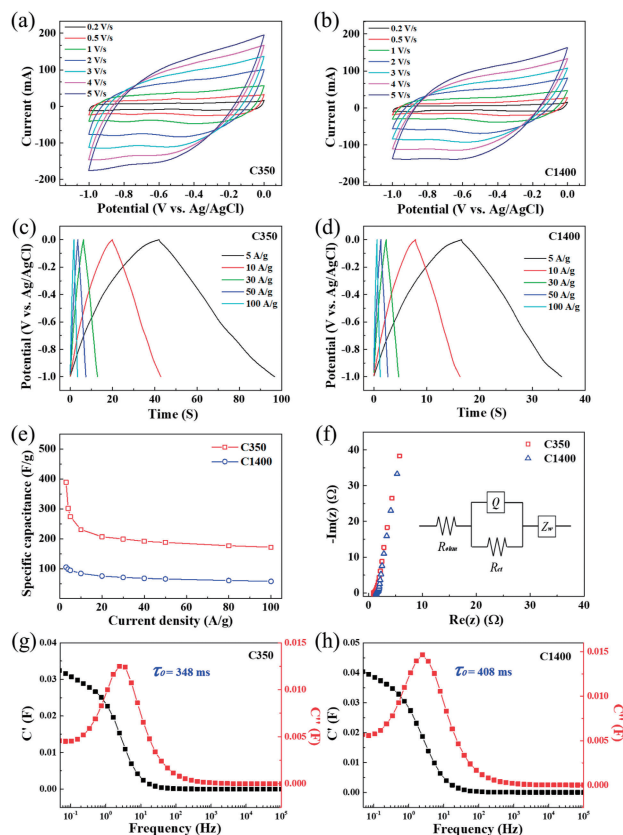


**Figure 3.** Electrochemical performances of C350 and C1400 samples in a three-electrode system. (a, b) CV curves of (a) C350 and (b) C1400, (c, d) GCD profiles of (c) C350 and (d) C1400, (e) specific capacitance variation with increase in the applied current density, (f) AC impedance plot of C350 and C1400 samples, and (g, h) relaxation times of C350 and C1400 electrodes, respectively.

potential range of  $-1.0$ – $0.0$  V, using scan rates from  $0.2$   $\text{V s}^{-1}$  to  $100$   $\text{V s}^{-1}$ . Galvanostatic discharge-charge (GDC) tests were conducted at the current densities from  $5$   $\text{A g}^{-1}$  to  $100$   $\text{A g}^{-1}$ . The electrochemical impedance spectra (EIS) were measured from  $10$  mHz to  $100$  kHz frequency with an amplitude of  $5$  mV.

The gravimetric capacitance ( $C_g$ ) was calculated by discharge profiles in the potential range using the following equation:

$$C_g = \frac{I \times t}{W \times \Delta U} \quad (1)$$

where  $I$  is the discharge current,  $t$  is the duration of discharge,  $W$  is the weight of the carbon materials on the electrode, and  $\Delta U$  is the potential window of the discharge process. This calculation was adopted in Figure 3c–d to obtain Figure 3e.

**Flexible Microsupercapacitor:** In the present study, solid electrolyte was used with the FSC. The solid electrolyte was formed by dropping liquid electrolyte onto the surface of as-deposited patterned PET substrate and drying in air, which was prepared by dissolving 3 g polyvinyl alcohol (PVA) and 3 g KOH in 30 ml distilled water at  $80$  °C for 2 h with vigorous stirring. CV measurements were carried out within a potential range of  $0.0$ – $0.8$  V (or  $0.0$ – $2.4$  V for 3 FSC devices in series) and the scan rates were set between  $0.2$   $\text{V s}^{-1}$  and  $10$   $\text{V s}^{-1}$ . The

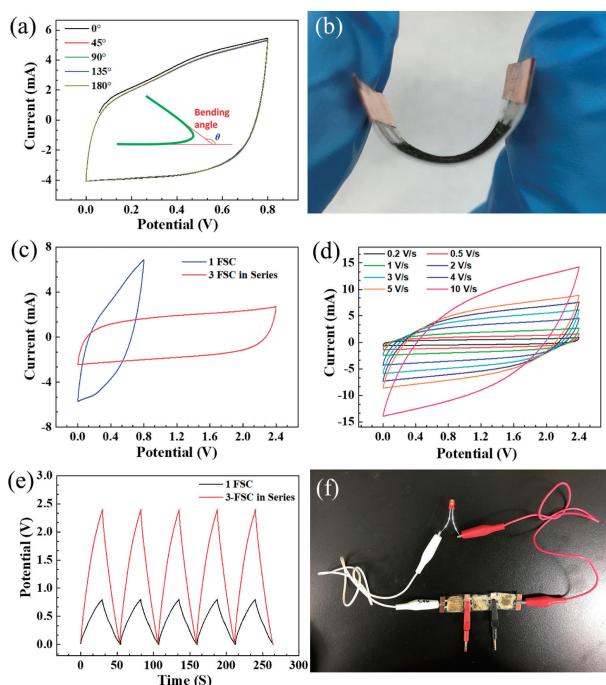


**Figure 4.** Electrochemical performances of FSC devices with C350 as active material in a two-electrode system. (a) CV curves of a single FSC device under different bending angles, (b) photograph of the bendable single FSC device, (c) CV curves of a single FSC device and 3 connected FSC devices in series with a scan rate of  $1 \text{ V s}^{-1}$ , (d) CV curves of 3 connected FSC devices in series at different scan rates from  $0.2 \text{ V s}^{-1}$  to  $10 \text{ V s}^{-1}$ , (e) GCD curves of a single FSC device and 3 connected FSC devices in series at a current density of  $0.14 \text{ mA cm}^{-2}$ , and (f) photograph of 3 connected FSC devices in series which can generate LED lighting.

volumetric capacitance ( $C_v$ ) was calculated by taking the integral of the cyclic voltammogram in the potential range using the following equation:

$$C_v = \frac{Q}{2V \times \Delta U} \quad (2)$$

where  $Q$  is the charge,  $V$  is the volume of the films deposited on the substrate, and  $\Delta U$  is the potential window. This calculation was used in Figure 4d to obtain Figure S2.

Under a given scan rate, the power density  $P_v$  was calculated by integrating the cyclic voltammogram plots. The energy density ( $E_v$ ) was calculated according to the following equations:

$$P_v = \int_0^{V_0} I \times U dv \quad (3)$$

$$E_v = \frac{P_v \times \Delta U}{v \times 3600} \quad (4)$$

where  $\Delta U$  is the potential window of the discharge process and  $v$  is the scan rate. This calculation was used in Figure 4d to obtain Figure S4.

### 3. Results and Discussion

The SEM morphologies of as-synthesized ZIF-8 particles and ZIF-8 derived carbon particles are presented in Figure 2a–h.

The size distributions of the particles are homogenous before and after the carbonization step. ZIF-8 particles in Figure 2a–b have particle sizes around 350 nm and demonstrate the typical rhombic dodecahedral shape of zeolitic imidazolate frameworks, thus implying successful morphology control in our synthesis of ZIF-8. When the mole ratio of  $\text{Zn}(\text{NO}_3)_2 \cdot 6\text{H}_2\text{O}$  and MIm is changed from 1:70 to 1:50, the size of ZIF-8 particles increases significantly to about 1400 nm and shows smoother surface morphology in Figure 2c–d. The images of carbonized particles are shown in Figure 2e–h, which preferentially keep original rhombic dodecahedron shape as ZIF-8 particles. The morphology of carbon particles seems to have slightly shrunk due to the structure variation during high-temperature treatment.

Figure 2i shows the XRD patterns of ZIF-8 and its derived carbon material. The diffraction peaks of ZIF-8 are all in good accordance with the simulated pattern of the ZIF-8 structure, which indicates high level of crystallization of as-prepared ZIF-8 particles without impurities. After carbonization at  $800^\circ\text{C}$  for 5 h, the diffraction peaks of ZIF-8 structure disappear and only amorphous peaks can be found at  $2\theta$  angle from  $20^\circ$  to  $30^\circ$ . From such amorphous peaks, it can be inferred that the ZIF-8 particles have been transformed to carbon particles. The graphitization degree of ZIF-8 derived carbon particles can be distinguished from Raman patterns in Figure 2j. The positions of  $D$  and  $G$  bands of C350 and C1400 are at about  $1348 \text{ cm}^{-1}$  and  $1599 \text{ cm}^{-1}$  wavenumbers. The  $D$  band is generally believed to represent the part of disordered or partially ordered structure in carbon materials, while  $G$  band has a relationship with the graphitization degree of carbon materials. The significant intensity of the  $G$  band indicates a high level of graphitic content and higher electrical conductivity. The relative intensity ratio of  $I_D/I_G$  are respectively equal to 0.99 and 1.00 for C350 and C1400 samples, suggesting that the disordered/amorphous carbon and graphitic carbon are co-existing.

The information on surface areas and pore size distribution of C350 and C1400 particles are studied *via* nitrogen adsorption-desorption isothermal method. In Figure S1a, adsorption-desorption isotherms of C350 and C1400 present well-overlapped shape during the process of nitrogen adsorption and desorption. There is no visible hysteresis loop. The pore size distribution of C350 and C1400 are displayed in Figure S1b. It can be seen that a majority of pores in both particles are micropores with diameter less than 2 nm, with only some mesopores ranging between 3 and 4 nm present in C350 particles. The surface area of C350 reaches  $754.15 \text{ m}^2 \text{ g}^{-1}$ , which is higher than  $684.14 \text{ m}^2 \text{ g}^{-1}$  of C1400. Furthermore, the pore volumes of C350 and C1400 are  $0.452 \text{ cm}^3 \text{ g}^{-1}$  and  $0.329 \text{ cm}^3 \text{ g}^{-1}$ , respectively. The C350 sample has a higher surface area and larger pore volume. This observation indicates that particle size influences the carbonization of ZIF-8 which ultimately affects porosity.

In Figure 3a–b, the CV curves under different scan rates from  $0.2 \text{ V s}^{-1}$  to  $5 \text{ V s}^{-1}$  are demonstrated. CV curves present similar rectangle shapes for both C350 and C1400, which are attributed to the double-layer capacitance of carbon materials. Although the outlines of CV curves tend to deviate gradually from rectangle shape at higher scan rates, the rectangle profiles of CV can be roughly maintained even at high scan rate. It

implies stable and typical capacitance performances of our carbon materials. Galvanostatic discharge-charge (GDC) curves under various current densities are presented in Figure 3c–d. The charge and discharge processes all show nearly linear profiles within  $-0.1$ – $0.0$  V (vs. Ag/AgCl), indicating typical capacitive properties of C350 and C1400 samples.

The GDC discharge duration of C350 and C1400 electrodes are 48 seconds and 18 seconds at a current density of  $5 \text{ A g}^{-1}$ , respectively. There is a apparent difference in discharge duration because the specific capacitance of the C350 material is nearly three times higher than C1400. The variation of discharge specific capacitance on current density is displayed in Figure 3e. At a smaller current density ( $<5 \text{ A g}^{-1}$ ), the C350 and C1400 materials achieve high specific capacitance (e.g.,  $389 \text{ F g}^{-1}$  and  $105 \text{ F g}^{-1}$ , respectively). The specific capacitances promptly decrease with the increase of current density. When the current density is greater than  $10 \text{ A g}^{-1}$ , the notable drop of the specific capacitances stop, and the curves reach near their plateaus. The specific capacitance of C350 remains  $178 \text{ F g}^{-1}$  even at a high current density of  $100 \text{ A g}^{-1}$ , which is more than three times than  $58 \text{ F g}^{-1}$  of C1400. Therefore, C350 material has high specific capacitance and outstanding capacitance retention capability at high current density.

EIS measurements were used to investigate the electrochemical properties of C350 and C1400 as active materials for supercapacitors. Figure 3f shows the Nyquist plots. The EIS curves can be well fitted with an equivalent circuit in the inset in Figure 3f.  $R_{ohm}$  represents the ohm resistance of electrolyte and connections in system *etc.*, and  $R_{ct}$  is the charge transfer resistance.  $Q$  is defined as a constant phase angle element due to the frequency response difference between real electrochemical double-layer capacitance and the theoretical maximum capacitance, which is utilized to simulate the capacitance properties of the electrode.  $Z_W$ , called Warburg impedance, has a relationship with the ion diffusion at low-frequency region. Both C350 and C1400 show straight lines with large slopes in the low-frequency region, which indicates excellent ion diffusion conditions during the electrochemical process.

The EIS data in Figure 3g–h show that the C350 carbon material has a shorter relaxation time ( $\tau_0$ ) of 348 ms than C1400 carbon material whose relaxation time is 408 ms. Minor relaxation time of active material is beneficial to the rapid charge-discharge process and to achieve excellent capacitance retention even under high current conditions, which corresponds well with the results in Figure 3e that both C350 and C1400 can keep stable capacitance up to  $100 \text{ A g}^{-1}$  current density. As a result, as-synthesized C350 and C1400 carbon materials are both quite suitable for acting as active electrode materials in supercapacitors due to their large surface area, massive micro/mesopores and short relaxation times. Especially, C350 carbon material has superior electrochemical performances than that of C1400 and will be used in following microsupercapacitor devices.

The FSC was fabricated according to the indicative size in Figure 1b. ZIF-8 derived carbon particles were successfully deposited on the patterned lines, as shown in Figure 1c–d. The interdigital finger outline of the electrode is beneficial to high capacitance generation and its electrochemical performance. The CV measurement results of the FSC indicate the expected

characteristics of a supercapacitor. The CV curves of the FSC under different bending angles are also shown in Figure 4a. The CV curves overlap to a large extent when the bending angle changes from  $0^\circ$  to  $180^\circ$ , indicating the excellent stability of as-prepared FSC under bending. The image of bending the FSC can be seen in Figure 4b. For flexible devices, the work abilities under bending or twisting conditions are the key to practical application.

To investigate the combined performance of the FSC, three pieces of the FSC are connected in series and electrochemically studied. The FSCs in series display stable electrochemical processes within the  $0.0$  to  $2.4$  V voltage range in CV and GDC measurements, as presented in Figure 4c–d and Figure 4e, respectively. With the scan rate varying from  $0.2 \text{ V s}^{-1}$  to  $10 \text{ V s}^{-1}$ , the shapes of CV curves still maintain a roughly symmetric rectangle. From CV measurements under different scan rates (Figure 4d), we calculated the volumetric capacitances of the FSC device, as shown in Figure S2. The volumetric capacitance of FSC gradually decreases as the scan rate increases. After connection of 3 FSC devices in series, the voltage windows are expanded to  $2.4$  V, while the capacitance drops to one third in comparison to a single FSC device according to the eq (2), which was observed previously.<sup>23</sup> Practically, the FSC in series can successfully light an LED in Figure 4f, which is an additional benefit obtained from the high voltage after connection in series. At the same time, the long cycling performance of FSC in Figure S3 indicates its potential for electrochemical applications. The Ragone plot of the FSC device in Figure S4 also reveals its good properties. Our FSC presents obvious advantages over other flexible devices.

#### 4. Conclusion

Microsupercapacitors with ZIF-8 derived carbon as active materials have been fabricated *via* a simple electrophoresis assembly method. This electrophoresis method is easy to control and thus able to provide a high-quality, uniform carbon material with high surface area and good electrical conductivity. We have investigated the performance of these carbon materials in microsupercapacitor devices. The flexible microsupercapacitors fabricated by electrophoresis also demonstrate excellent electrochemical performance. Based on the simplicity and convenience of the film making process and excellent electrochemical properties, microsupercapacitors described here are good candidate materials for future miniaturized or flexible power supplies.

This research was supported by the Principal Research Program (PNK5600) at the Korea Institute of Materials Science (KIMS).

#### Supporting Information

This material is available on <https://doi.org/10.1246/bcsj.20190298>.

#### References

- # These authors equally contributed to this work.
- 1 Z. Ren, Y. Chang, Y. Ma, K. Shih, B. Dong, C. Lee, *Adv. Opt. Mater.* **2019**, 1900653.
- 2 D. Fahimi, O. Mahdavi-pour, J. Sabino, R. M. White, I.

- Paprotny, *Sens. Actuators, A* **2019**, *299*, 111569.
- 3 K. Noi, A. Iwata, F. Kato, H. Ogi, *Anal. Chem.* **2019**, *91*, 9398.
  - 4 B. Ji, M. Wang, C. Ge, Z. Xie, Z. Guo, W. Hong, X. Gu, L. Wang, Z. Yi, C. Jiang, B. Yang, X. Wang, X. Li, C. Li, J. Liu, *Biosens. Bioelectron.* **2019**, *135*, 181.
  - 5 H. Hosseinzadegan, O. N. Pierron, E. Hosseinian, *Sens. Actuators, A* **2014**, *216*, 342.
  - 6 H. Zhang, Y. Cao, M. O. L. Chee, P. Dong, M. Ye, J. Shen, *Nanoscale* **2019**, *11*, 5807.
  - 7 Z.-S. Wu, K. Parvez, X. Feng, K. Müllen, *Nat. Commun.* **2013**, *4*, 2487.
  - 8 S. Makino, Y. Yamauchi, W. Sugimoto, *J. Power Sources* **2013**, *227*, 153.
  - 9 M. Beidaghi, C. Wang, *Adv. Funct. Mater.* **2012**, *22*, 4501.
  - 10 C. Largeot, C. Portet, J. Chmiola, P.-L. Taberna, Y. Gogotsi, P. Simon, *J. Am. Chem. Soc.* **2008**, *130*, 2730.
  - 11 W. Xing, S. Z. Qiao, R. G. Ding, F. Li, G. Q. Lu, Z. F. Yan, H. M. Cheng, *Carbon* **2006**, *44*, 216.
  - 12 Q. Lu, J. G. Chen, J. Q. Xiao, *Angew. Chem., Int. Ed.* **2013**, *52*, 1882.
  - 13 C. Costentin, T. R. Porter, J. M. Savéant, *ACS Appl. Mater. Interfaces* **2017**, *9*, 8649.
  - 14 H. C. Zhou, J. R. Long, O. M. Yaghi, *Chem. Rev.* **2012**, *112*, 673.
  - 15 N. Stock, S. Biswas, *Chem. Rev.* **2012**, *112*, 933.
  - 16 B. Liu, H. Shioyama, T. Akita, Q. Xu, *J. Am. Chem. Soc.* **2008**, *130*, 5390.
  - 17 H. B. Aiyappa, P. Pachfule, R. Banerjee, S. Kurungot, *Cryst. Growth Des.* **2013**, *13*, 4195.
  - 18 W. Chaikittisilp, K. Ariga, Y. Yamauchi, *J. Mater. Chem. A* **2013**, *1*, 14.
  - 19 M. Hu, J. Reboul, S. Furukawa, N. L. Torad, Q. Ji, P. Srinivasu, K. Ariga, S. Kitagawa, Y. Yamauchi, *J. Am. Chem. Soc.* **2012**, *134*, 2864.
  - 20 Y. V. Kaneti, J. Tang, R. R. Salunkhe, X. Jiang, A. Yu, K. C. Wu, Y. Yamauchi, *Adv. Mater.* **2017**, *29*, 1604898.
  - 21 W. Chaikittisilp, M. Hu, H. Wang, H. S. Huang, T. Fujita, K. C. Wu, L. C. Chen, Y. Yamauchi, *Chem. Commun.* **2012**, *48*, 7259.
  - 22 H. L. Jiang, B. Liu, Y. Q. Lan, K. Kuratani, T. Akita, H. Shioyama, F. Zong, Q. Xu, *J. Am. Chem. Soc.* **2011**, *133*, 11854.
  - 23 Y. Wang, Y. Shi, C. X. Zhao, J. I. Wong, X. W. Sun, H. Y. Yang, *Nanotechnology* **2014**, *25*, 094010.